TÜBİTAK

Turkish Journal of Earth Sciences

http://journals.tubitak.gov.tr/earth/

Research Article

Turkish J Earth Sci
(2013) 22: 220-238
© TÜBİTAK
doi:10.3906/yer-1202-1

Coeval Shoshonitic-ultrapotassic dyke emplacements within the Kestanbol Pluton, Ezine – Biga Peninsula (NW Anatolia)

Cüneyt AKAL*

Dokuz Eylül University, Engineering Faculty, Department of Geological Engineering, Tınaztepe - Buca TR-35160 İzmir, Turkey

Received: 01.02.2012 • **Accepted:** 20.05.2012 • **Published Online:** 27.02.2013 • **Printed:** 27.03.2013

Abstract: The Biga Peninsula, in the north-western part of Western Anatolia, is part of the Sakarya Zone of the Western Pontides and the tectonically overlying Ezine group. The basement rocks are intruded by the early Miocene Kestanbol Pluton and early to middle Miocene calc-alkaline to shoshonitic-ultrapotassic volcanic successions related to postcollisional continental extension. The Kestanbol Pluton mainly comprises monzonite and granodiorite and is cut by shoshonitic-ultrapotassic tephriphonolite dykes. ^{40}Ar-^{39}Ar ages of biotite (21.22 ± 0.09 Ma) and leucite (22.21 ± 0.07 Ma) crystals indicate that tephriphonolite dyke emplacement was coeval with the intrusion of the Kestanbol Pluton during the early Miocene (21.5 ± 1.6, 22.8 ± 0.2 Ma). The geochemical features of the tephriphonolite dykes suggest a phlogopite-bearing mantle source which may originate from a previously metasomatised subcontinental lithospheric mantle source. This mantle source shows the imprints of carbonate-reach oceanic sediment recycling and crustal material contamination processes, which evolved during northward subduction and closure of the northern branch of the Neo-Tethys Ocean beneath the Sakarya zone during the late Cretaceous to Eocene.

Key Words: Western Anatolia, Biga Peninsula, Sakarya Zone, Neo-Tethys, tephriphonolite, leucite, coeval dyke emplacement

1. Introduction

The complex geological structure of Anatolia was shaped by the opening and closing of the Palaeo- and Neo-Tethys oceans from the Early Palaeozoic to the Tertiary. During the Palaeo-Tethyan stage, the Anatolide-Tauride platform was rifted from the northern margin of Gondwana, causing the opening of the northern branch of the Neo-Tethys Ocean (Şengör & Yılmaz 1981; Akal *et al.* 2011, 2012). The northward movement of the Anatolide-Tauride platform led to accretion and Late Cretaceous – Early Tertiary continental collision with the Pontide belt, which has Laurasian affinity (Şengör & Yılmaz 1981; Okay *et al.* 1996, 2006; Göncüoğlu & Kozlu 2000; Stampfli 2000; Göncüoğlu *et al.* 2007). Subduction of the northern branch of Neo-Tethys ended with continent–continent collision and the development of the İzmir-Ankara-Erzincan suture zone of Turkey (Brinkmann 1966; Ketin 1966; Okay & Tüysüz 1999; Aldanmaz *et al.*, 2000).

The Biga Peninsula is located north of the İzmir-Ankara-Erzincan suture zone. It represents the westernmost segment of the Pontides. The major tectonic units of the peninsula consist, from north to south, of the Sakarya zone and the tectonically overlying Ezine group (Okay & Tüysüz 1999; Beccaletto & Jenny 2004) (Figures 1 and 2). The basement of the peninsula is intruded by early to middle Miocene plutonic and volcanic rocks and related volcanoclastic sequences (Birkle & Satır 1995; Ercan *et al.* 1995; Aldanmaz *et al.* 2000). This magmatism in the Biga Peninsula is related to Late Cretaceous to Eocene northward subduction of the northern Neo-Tethys Ocean beneath the Sakarya continent, resulting in final collision between the Sakarya continent and the Anatolide-Tauride platform (Borsi *et al.* 1972; Ercan *et al.* 1995; Şengör & Yılmaz 1981; Yılmaz 1989, 1990, 1997; Yılmaz *et al.* 2001; Karacık & Yılmaz 1998; Harris *et al.* 1994). Eocene magmatism is represented by granitic plutons and their volcanic equivalents (e.g., Altunkaynak & Dilek 2006; Altunkaynak *et al.* 2012). In the early Miocene, postcollisional magmatic activity produced high-K calc-alkaline to shoshonitic, I-type plutonic rocks (Kestanbol Pluton: 21.5 ± 1.6 Ma, Birkle & Satır 1995; 22.3 ± 0.2 Ma and 22.8 ± 0.2 Ma, Altunkaynak *et al.* 2012) and coeval calc-alkaline and shoshonitic volcanic rocks (Karacık 1995; Birkle & Satır 1995; Karacık & Yılmaz 1998; Aldanmaz *et al.* 2000). This magmatic episode is related to postcollisional continental extension (Yılmaz 1997; Karacık & Yılmaz 1998; Aldanmaz *et al.* 2000, 2006; Yılmaz *et al.* 2001). Late-stage magmatism on the Biga peninsula is represented by Na-rich alkaline volcanism (Aldanmaz *et al.* 2000, 2006), which postdates the early Miocene episode.

* Correspondence: cuneyt.akal@deu.edu.tr

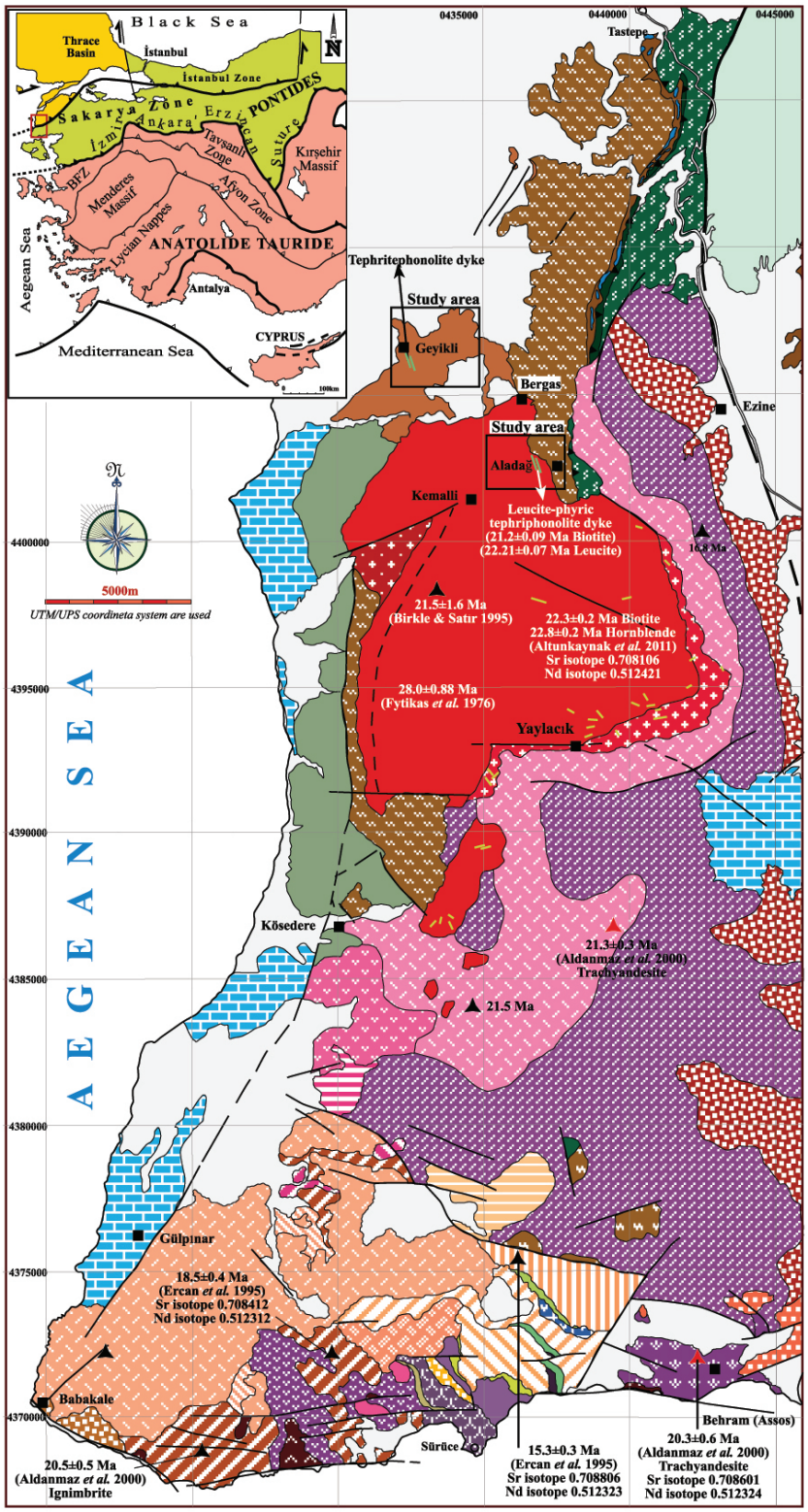


Figure 1. Distribution of shoshonitic-ultrapotassic dykes on the Biga Peninsula. Detailed geological map of plutonic and volcanic rock units of the Biga Peninsula are from Karacık (1995); Karacık & Yılmaz (1998). Geological map of basement rock units and ages are from Kalafatçıoğlu (1963); Fytikas *et al.* (1976); Okay *et al.* (1991); Birkle & Satır (1992, 1995); Ercan *et al.* (1995); Okay & Tüysüz (1999); Aldanmaz *et al.* (2000); Okay & Satır (2000); Beccaletto & Jenny (2004); Altunkaynak & Genç (2008) and Yılmaz-Şahin *et al.* (2010). Legend and explanation of the rock units are given in Figure 2.

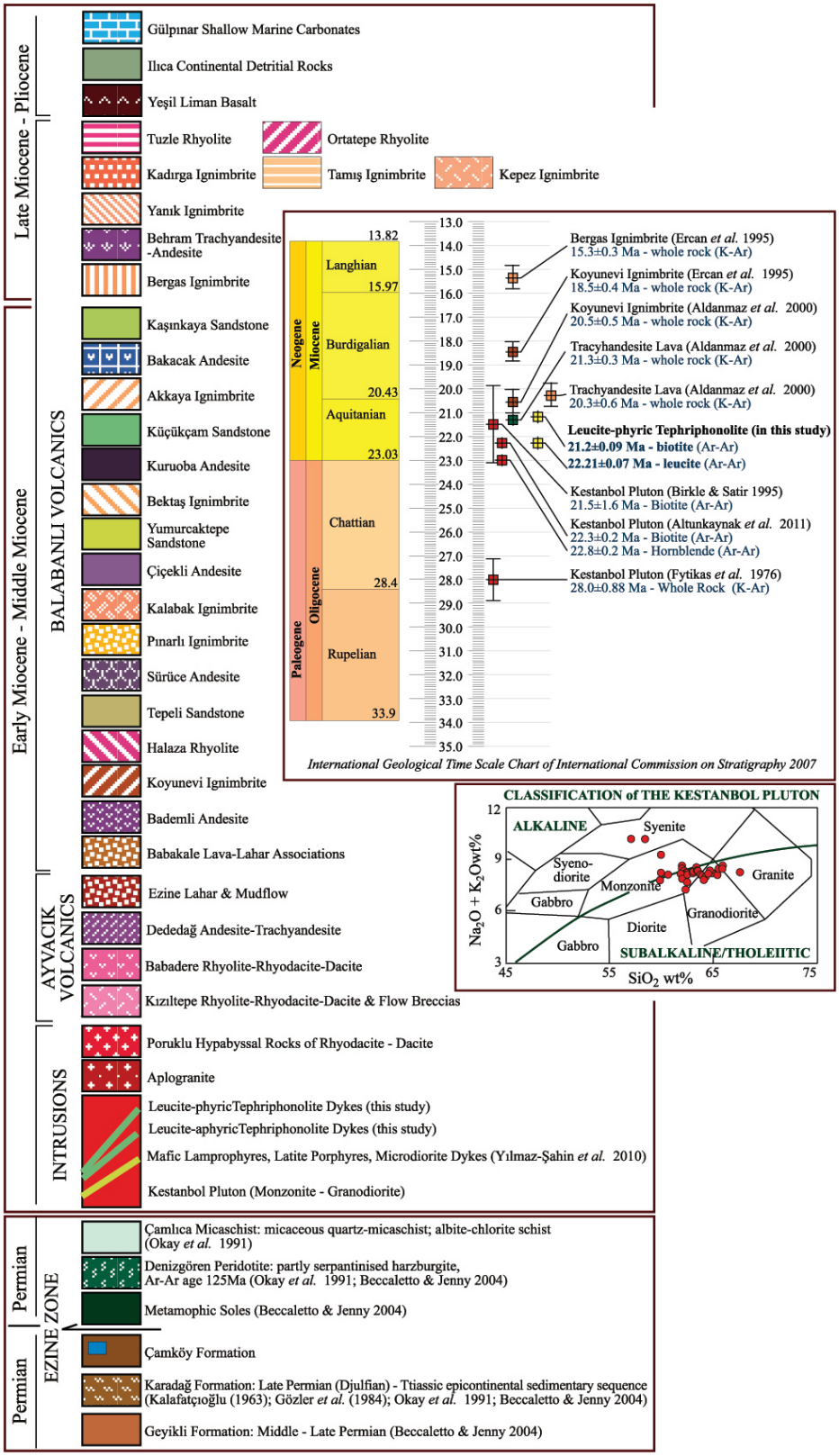


Figure 2. Geological units of the Biga Peninsula and geochronological age frame for the igneous rocks. The Kestanbol Pluton mainly occupies the monzonite and granodiorite fields and also plots in the granite and syenite fields on the alkali vs. silica diagram of Cox *et al.* (1979). Data are from Karacık & Yılmaz (1998), Yılmaz-Şahin *et al.* (2010) and Altunkaynak *et al.* (2012).

The Kestanbol Pluton covers an area of about 125 km^2 (Karacık & Yılmaz 1998; Yılmaz-Şahin *et al*. 2010). It has a medium- to fine-grained hypabyssal zone, which shows a gradual transition into the main plutonic body toward the eastern border (Figures 1 and 2). The hypabyssal zone passes gradually into rhyodacitic and dacitic rocks, and was interpreted to indicate emplacement of the pluton into its coeval subvolcanic volcanic ejecta (Karacık & Yılmaz 1998; Aldanmaz *et al*. 2000). The pluton contains mafic microgranular enclaves and mafic vein rocks, which are described by Yılmaz-Şahin *et al*. (2010) as lamprophyre, leucite porphyry and microdiorite. Mafic microgranular enclaves, lamprophyres, leucite porphyries and microdiorite dykes show mixing and mingling relationships with the monzonitic to granodioritic magma (Yılmaz-Şahin *et al*. 2010), indicating that the Kestanbol Pluton formed by mixing of mantle-derived mafic magmas and melts of granodioritic composition (Altunkaynak & Genç, 2008; Yılmaz-Şahin *et al*. 2010). In a recent study, Altunkaynak *et al*. (2012) suggest that slab breakoff-related asthenospheric upwelling led to underplating of mantle-derived magmas. This process provided the heat necessary to induce partial melting of lithospheric mantle, resulting in the production of the Oligo-Miocene I-type granitoid magmas.

This paper presents new mineralogical and geochemical data as well as the first high-precision Ar-Ar geochronological data for leucite phenocryst-bearing Si-undersaturated shoshonitic to ultrapotassic dykes cutting the Kestanbol Pluton. The aim is additionally to constrain the mingling and mixing features with the coeval Kestanbol Pluton during postcollisional, orogenic magmatism on the Biga Peninsula. Using trace element data to assess the mantle enrichment processes, the origin of this shoshonitic to ultrapotassic magma is discussed in light of the carbonate-bearing oceanic sediment recycling and crustal contamination within the previously metasomatised subcontinental lithospheric mantle source. My main conclusion is that these lavas were derived by melting of crustally contaminated mantle similar to, but subtly distinct from, the mantle source later tapped during late Miocene-Pliocene Western Anatolian magmatism.

2. Analytical Techniques

Whole-rock major, trace and rare earth element analyses of 10 fresh samples were conducted by ICP-emission spectrometry (Jarrel Ash AtomComp Model 975, Spectro Ciros Vision) and ICP-mass spectrometry (Perkin-Elmer Elan 6000 or 9000) at ACME Analytical Laboratories, Vancouver, British Columbia, Canada. Whole-rock powders were obtained by crushing and splitting from rock samples of about 5 kg. As much as possible, K-feldspar xenocrysts were removed from the rock pieces by hand-picking. All samples were milled using a tungsten carbide disc-mill (Retsch RS100; average milling time was 2 minutes).

$^{40}Ar/^{39}Ar$ incremental heating experiments were conducted on biotite and leucite separates at the IFM-GEOMAR Tephrochronology Laboratory. After crushing and sieving, the particles were hand-picked from the 100-300 µm size fraction. Resulting mineral separates and chips were cleaned using an ultrasonic disintegrator. Phenocrysts were then etched in 15% hydrofluoric acid for 10 minutes. Samples were neutron irradiated at the 5 MW reactor of the GKSS Reactor Center (Geesthacht, Germany), with crystals and matrix chips in aluminium trays and irradiation cans wrapped in 0.7 mm of cadmium foil. Samples were step-heated by laser. Purified gas samples were analysed using a MAP 216 noble gas mass spectrometer. Raw mass spectrometer peaks were corrected for mass discrimination, and background and blank values determined every fifth analysis. The neutron flux was monitored using TCR sanidine (Taylor Creek Rhyolite = 27.92 Ma) (Dalrymple & Duffield 1988) and internal standard SAN6165 (0.470 Ma; Van den Bogaard 1995). Vertical variations in J values were quantified by a cosine function fit. Lateral variations in J were not detected. Corrections for interfering neutron reactions on Ca and K are based on analyses of optical grade CaF_2 and high-purity K_2SO_4 salt crystals that were irradiated together with the samples. Ages derived from step-heating analyses are based on plateau portions of the age spectra. Plateau regions generally comprise >50% of the ^{39}Ar released and more than 3 consecutive heating steps that yield the same ages (within 2σ error).

3. Geological setting

Two distinct dyke types can be distinguished within the Kestanbol Pluton and its surrounding country rocks: 1) leucite-bearing tephriphonolite (formerly mapped as (?) leucite porphyry) and 2) leucite-free tephriphonolite (formerly classified as lamprophyre). The dykes are randomly distributed throughout the pluton and the country rocks; their thickness varies between 0.5 to 10 m (Figure 1). Dyke distribution within the pluton was mapped by Yılmaz-Şahin *et al*. (2010). Fine-grained dark green and brown leucite phenocryst-free tephriphonolite dykes and greenish grey leucite-bearing tephriphonolite dykes, with pseudoleucite crystals reaching up to 1.5 cm across, are well exposed on road cuts south of Geyikli town and west of Aladağ village. The tephriphonolite dykes near Geyikli intruded recrystallised detrital limestone lens-bearing metashales of the Geyikli Formation (Beccaletto & Jenny 2004; Yaltırak & Okay 2004) of the Ezine group (Figure 3a). A sharp contact was noticed between the dykes and the country rocks without any contact

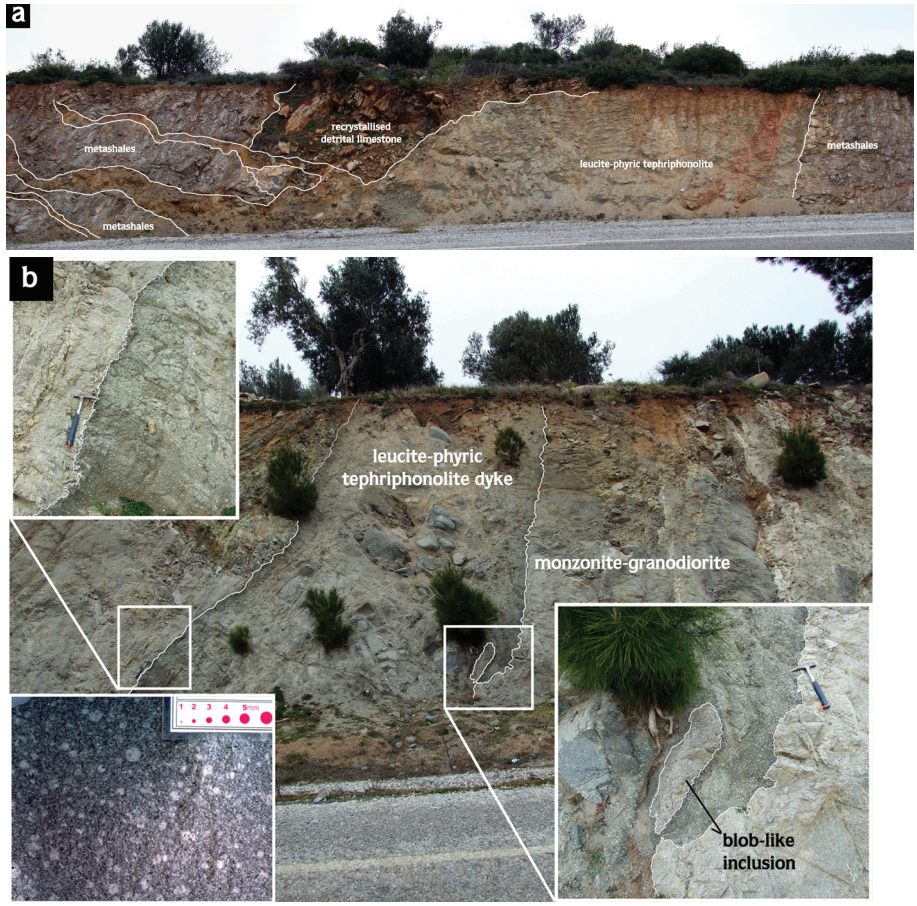


Figure 3. (a) Road cut near Geyikli town (35 S 0432577 - 4406273) exposing sills of leucite-phyric tephriphonolite. **(b)** Dyke of leucite-phyric tephriphonolite with lobate (curved) contact and blob-like inclusion of monzonitic-granodioritic host rock (35 S 0437234 - 4402918).

metamorphic effects. Along the contact chilled margins or glassy structures were not developed.

Both dyke types show the same contact relationship with the Kestanbol Pluton (Figures 3b, 4a, and 4b). They have lobate (curved) margins towards the host rocks (Figures 3b and 4b), indicating that granites and dykes were at least partially molten at the time of intrusion. Both dyke types contain orthoclase xenocrysts and blob-like inclusions of monzonite-granodiorite near the contacts, indicating magma mingling and mixing (such inclusions, however, may also indicate wall-rock assimilation at lower temperatures) relationships between the dykes and the coeval monzonite-granodiorite (Figures 3b and 4c). The macro- and micro-textures along the contact provide additional evidence for the near-simultaneity between the intrusion of the dykes and monzonitic-granodioritic magma.

4. Petrography

The fine-grained leucite-free and leucite-bearing tephriphonolite dykes show porphyritic textures with macrocrysts of clinopyroxene, biotite, orthoclase and plagioclase (Figures 5a-5c). Most of the biotite crystals are completely pseudomorphed by chlorite. Plagioclase is largely replaced by a mixture of sericite and epidote (Figure 5a). Large crystals of orthoclase and plagioclase are xenocrysts (0.5-1 cm) derived from the monzonite-granodiorite magma (Figure 4c). They were transferred and trapped by magma mixing or mingling in the shoshonitic-ultrapotassic magma during interaction with the monzonitic-granodioritic host. The aphanitic groundmass of the dykes contains prismatic clinopyroxene microcrysts, abundant biotite and plagioclase. Apatite occurs as widely scattered fine-grained euhedral grains as an accessory mineral.

The leucite phenocryst-bearing tephriphonolite dykes have seriate to highly porphyritic textures with euhedral leucite crystals up to 1.5 cm in length. Leucite, which makes up 30% of the rock, can be completely replaced by pseudomorphous K-feldspar (Figure 6a). The leucite phenocryst-bearing tephriphonolite dykes contain macrocrysts and microphenocrysts of euhedral

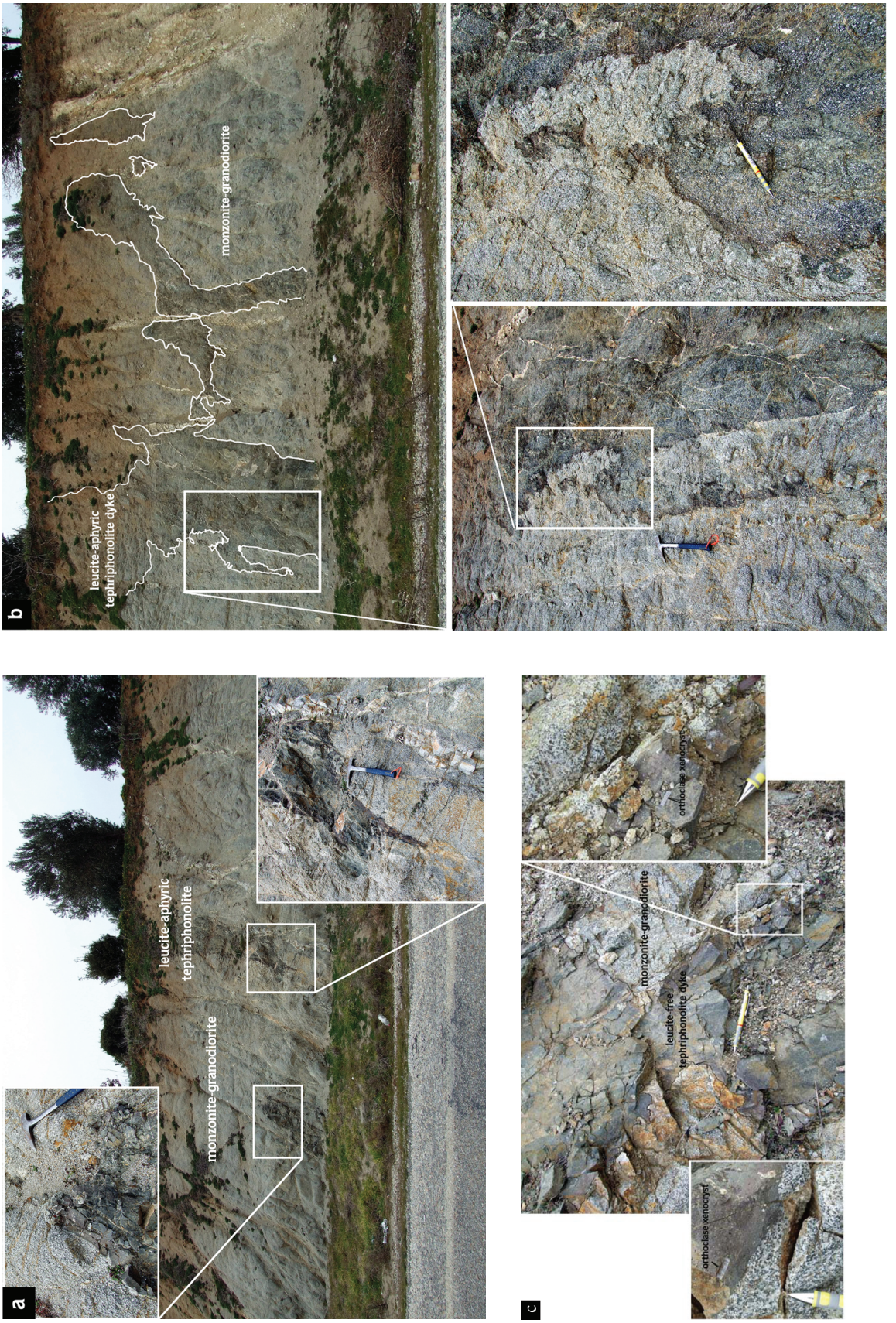


Figure 4. (a & b) Leucite-aphyric tephriphonolite dykes with well-developed lobate (curved) contact with monzonite-granodiorite indicating that the tephriphonolite was injected into the monzonitic-granodioritic magma before it was completely crystallised (35 S 0437290 - 4402974). **(c)** Orthoclase xenocrysts of monzonite-granodiorite in dyke, indicating that both types of igneous rocks were liquid at virtually the same time.

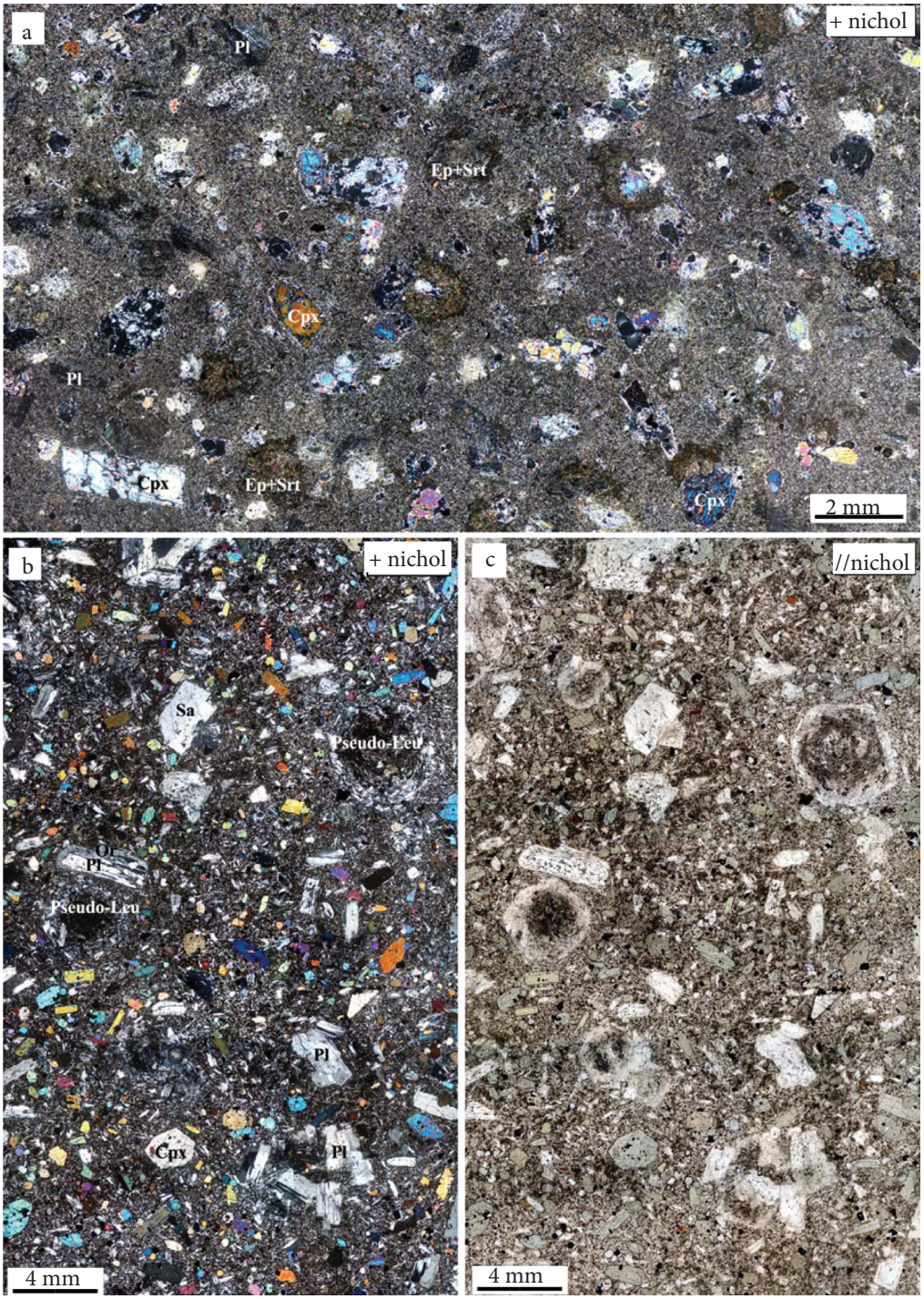


Figure 5. Photomicrography of **(a)** leucite-aphyric tephriphonolite and **(b & c)** leucite-phyric tephriphonolite dykes. Bt: biotite, Cpx: clinopyroxene, Ep: epidote, Leu: leucite, Or: orthoclase, Pl: plagioclase, Srt: sericite.

clinopyroxene (up to 5 mm), olivine, biotite and xenocrysts of orthoclase and plagioclase. Essential groundmass minerals are prismatic clinopyroxene, biotite, plagioclase, stubby apatite and opaque microcrysts. Clinopyroxene forms euhedral crystals with inclusions of apatite and opaque phases (Figures 6b and 6c). Polysynthetic twinned plagioclase is generally mantled by orthoclase (antirapakivi mantling) and this texture probably resulted from magma mixing between a monzonitic-granodioritic and a shoshonitic melt (Figure 6d). Olivine occurs as

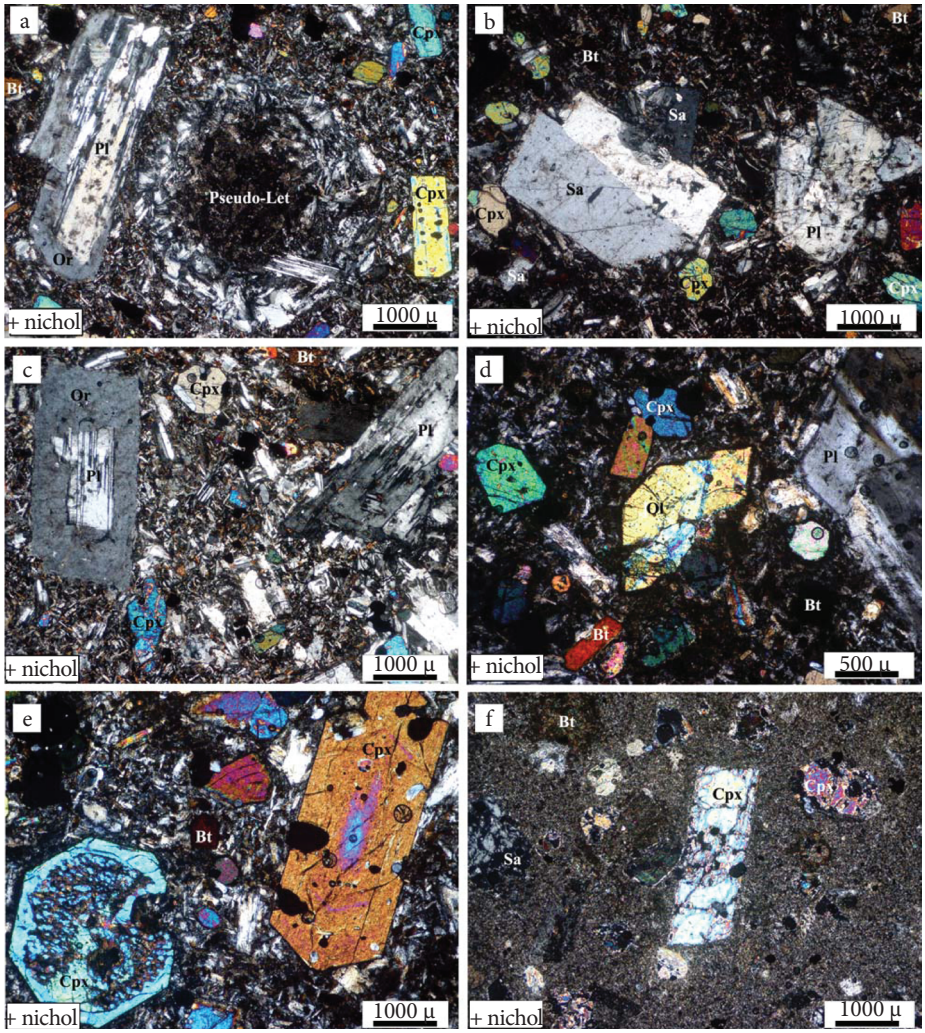


Figure 6. **(a)** Euhedral leucite replaced by pseudomorphous K-feldspar. **(b)** Spongy (sieve) clinopyroxene and optically zoned clinopyroxene phenocrysts in leucite-phyric tephriphonolites. **(c)** Euhedral clinopyroxene, plagioclase phenocrysts in aphanitic groundmass of leucite-aphyric tephriphonolite dykes. **(d)** Antirapakivi mantling on plagioclase phenocrysts. **(e)** Olivine microcryst with opaque mineral inclusions in the rims. The lath shaped brown crystals are biotite. **(f)** Orthoclase xenocrysts in seriate groundmass. Bt: biotite, Cpx: clinopyroxene, Pl: plagioclase, Ol: olivine, Leu: leucite, Or: orthoclase.

subhedral colourless microcrysts in the groundmass (containing up to 2%) and is easily distinguished by rims of opaque mineral inclusions (Figure 6e). Biotite forms dark brown lath-shaped or light brown and blade-shaped microphenocrysts (Figures 6e and 6f). Orthoclase xenocrysts are anhedral and display Carlsbad twinning (Figure 6f).

5. Geochemistry

Whole-rock major- and trace-element compositions are given in Table 1. Both dyke types belong to the shoshonitic magma series and are ultrapotassic, with ($K_2O/Na_2O > 2$ and $MgO > 3$), low silica (49.1 to 52.6 wt%) and high K_2O contents (5.2 to 7.3 wt%) (Figures 7a and 7b). Samples have high concentrations of Na_2O+K_2O, ranging from 8.4 to 11.5 wt%, and a concomitant increase of MgO from 2.8 to 4.2 wt%. Leucite phenocryst-bearing dykes are Si-undersaturated, as can be seen from the presence of normative nepheline and lack of normative quartz. CaO contents of the dykes vary between 5.4 and 7.6 wt%. TiO_2 contents are low, ranging from 0.7 wt% to 1.1 wt%. Mg numbers (Mg# = molar $Mg/(Mg + Fe_t)$) range from 43 to 50. The rocks also have low Ni contents (<36 ppm). Leucite-free and leucite-bearing dykes mainly fall in the tephriphonolite field in the TAS-IUGS diagram (Le Bas *et al.* 1986) and 2 of the leucite-free samples plot in the

Table 1. Major and trace element analyses of representative samples of leucite-phyric (LB) and leucite-aphyric (LF) tephriphonolite dykes. Chondrite and N-type MORB normalised values are from Sun & McDonough (1989).

Rock Type	Leucite-Phyric Dykes						Leucite-Aphyric Dykes						
Sample No	LB 07EZ02	LB 2254/12	LB 2255/1	LB 2255/2	LB 2254/4	LB 2254/9	LF 2254/3	LF 2254/6	LF 2254/7	LF 2254/8	LF 2254/10	LF 2254/11	LF 07EZ01
SiO_2	52.29	52.65	52.23	52.33	52.64	51.56	51.45	50.97	51.51	49.07	51.65	51.97	51.56
Al_2O_3	18.74	18.43	18.22	17.99	18.33	17.67	16.74	15.69	15.50	15.85	15.46	13.65	16.18
Fe_2O_3T	5.77	5.86	6.17	6.11	5.88	6.79	6.85	6.70	6.54	6.52	6.72	5.82	7.07
MgO	2.82	2.87	2.90	3.21	2.87	2.67	4.23	3.57	3.32	3.57	3.94	3.82	4.63
CaO	5.55	5.70	5.38	5.67	5.70	5.78	7.49	6.16	6.07	7.26	6.65	6.96	7.60
Na_2O	4.17	4.08	4.71	4.64	4.08	2.24	2.54	3.86	4.00	3.62	4.42	3.14	2.49
K_2O	6.80	6.68	6.76	6.55	6.68	7.29	6.06	6.07	6.04	5.21	5.15	6.11	5.93
TiO_2	0.72	0.70	0.71	0.74	0.70	0.81	0.86	0.87	0.84	0.82	0.84	1.11	0.86
P_2O_5	0.51	0.53	0.52	0.54	0.53	0.63	0.63	0.50	0.48	0.59	0.49	0.56	0.65
MnO	0.13	0.13	0.13	0.13	0.13	0.12	0.12	0.16	0.13	0.11	0.13	0.10	0.13
Cr_2O_3	0.01	0.01	0.01	0.01	0.01	0.01	0.01	0.01	0.01	0.01	0.01	0.02	0.01
LOI	1.9	1.8	1.4	1.3	1.8	3.8	2.4	4.9	5.0	6.9	4.0	6.2	2.3
Total	99.41	99.44	99.14	99.22	99.35	99.37	99.38	99.46	99.44	99.53	99.46	99.46	99.41
Ba	1767	1722	1636	1762	1986	2113	2288	2121	2033	1703	1856	1704	2055
Ni	10.9	11.6	14.5	16.2	10.1	15.1	23.2	25.4	21.4	20.6	23.1	35.6	23.5
Sc	12	12	13	14	12	14	20	17	16	19	17	19	23
Co	23.4	27.6	32.3	34.9	27.2	26.2	39.0	30.0	27.2	23.5	25.4	21.7	27.7
Ga	18.9	19.0	18.5	19.2	19.6	18.9	18.4	17.3	17.4	16.5	17.5	17.4	18.2
Nb	33.9	36.0	36.8	37.1	37.5	30.2	20.2	23.9	22.0	19.2	21.8	24.8	19.4
Rb	248.7	260.2	249.4	238.4	263.4	260.4	302.3	330.9	307.4	275.1	262.1	257.6	296.6
Sr	1223.7	1216.6	1204.4	1228.9	1261.9	1476.3	1210.3	1129.2	1162.8	957.5	1220.7	725.9	1088.1
Th	97.2	109.0	106.9	113.5	110.4	91.7	52.3	74.4	70.8	50.5	71.4	60.4	50.3
U	28.5	31.6	31.1	34.3	31.0	21.8	14.5	18.4	17.9	13.8	17.4	13.2	14.2
V	127	135	144	143	136	160	186	161	146	159	151	146	182
Zr	502.0	532.6	538.6	543.8	540.8	458.3	347.4	368.7	353.8	329.5	346.8	465.6	332.7
Y	25.1	26.5	27.5	27.9	27.0	31.2	27.0	29.9	28.4	25.2	28.2	26.1	27.1
Cu	58.3	62.9	62.4	62.8	59.5	69.1	74.6	30.4	36.3	62.5	36.4	10.9	68.9
Pb	95.1	98.7	82.4	79.6	98.3	76.7	23.2	33.8	55.4	33.4	38.6	26.2	32.0
Zn	38.0	39.0	38.0	38.0	37.0	57.0	84.0	72.0	64.0	43.0	46.0	48.0	78.0
Cs	16.8	16.8	16.9	15.7	18.7	7.4	23.8	42.5	35.9	28.7	34.5	10.6	25.8
Hf	11.8	11.9	12.6	12.3	12.9	10.7	8.4	8.7	8.8	8.2	9.1	14.1	9.2
Tl	0.6	0.6	0.7	0.6	0.6	0.3	1.6	3.4	3.1	1.9	2.4	0.6	1.7
W	98.2	154.6	198.8	192.3	143.5	99.5	133.0	104.1	107.8	36.9	59.6	57.6	43.4
Ta	2.4	2.3	2.5	2.3	2.6	2.0	1.4	1.6	1.7	1.4	1.6	2.0	1.4
La	103.6	106.2	110.7	107.8	116.2	110.1	79.2	93.6	95.1	72.6	92.4	88.3	76.5
Ce	203.5	209.3	216.6	211.5	224.8	216.0	160.7	184.5	188.0	152.8	183.7	206.7	161.2
Pr	20.4	21.5	22.1	23.0	22.2	23.6	18.4	20.3	19.6	17.6	19.7	24.4	18.5
Nd	71.8	76.6	78.5	83.5	82.1	90.6	74.9	75.1	75.6	68.0	75.8	100.5	76.2
Sm	11.7	12.2	12.5	12.6	12.9	13.7	12.3	12.7	12.4	11.4	12.4	16.5	12.8
Eu	2.5	2.6	2.7	2.9	2.7	3.2	2.7	2.7	2.6	2.6	2.7	3.0	2.9
Gd	8.3	8.5	9.2	8.9	8.9	10.1	9.0	9.1	9.2	8.4	9.2	10.6	9.3
Tb	1.0	1.1	1.1	1.2	1.1	1.3	1.1	1.2	1.2	1.1	1.2	1.2	1.2
Dy	4.8	5.2	5.6	5.3	5.1	5.8	5.2	5.7	5.7	4.9	5.4	5.4	5.4
Ho	0.8	0.8	0.9	1.0	0.9	1.1	0.9	1.0	0.9	0.9	0.9	0.8	0.9
Er	2.2	2.3	2.4	2.6	2.3	2.8	2.2	2.5	2.5	2.2	2.5	2.2	2.6
Tm	0.3	0.3	0.3	0.3	0.4	0.5	0.3	0.4	0.4	0.4	0.4	0.3	0.3
Yb	2.0	2.2	2.3	2.2	2.2	2.3	2.0	2.4	2.3	1.9	2.2	2.0	2.0
Lu	0.3	0.3	0.3	0.3	0.4	0.5	0.3	0.4	0.4	0.4	0.4	0.3	0.3
Mg#	48.1	48.1	47.1	49.9	48.0	42.7	53.9	50.2	49.0	50.9	52.6	55.4	55.4
$(La/Yb)_{CN}$	36.8	35.4	34.7	35.5	38.6	34.8	28.8	28.6	29.5	27.0	29.9	31.8	27.0
$(Ce/Sm)_{CN}$	4.3	4.3	4.3	4.2	4.4	3.9	3.3	3.6	3.8	3.4	3.7	3.1	3.1
$(Tb/Yb)_{CN}$	2.3	2.2	2.2	2.4	2.4	2.7	2.5	2.3	2.3	2.6	2.4	2.7	2.7
$(Nb/Yb)_{NM}$	21.97	21.92	21.04	22.28	22.73	17.42	13.42	13.31	12.47	13.02	12.85	16.31	12.51
Eu/Eu*	0.8	0.8	0.8	0.8	0.8	0.8	0.8	0.8	0.7	0.8	0.8	0.7	0.8

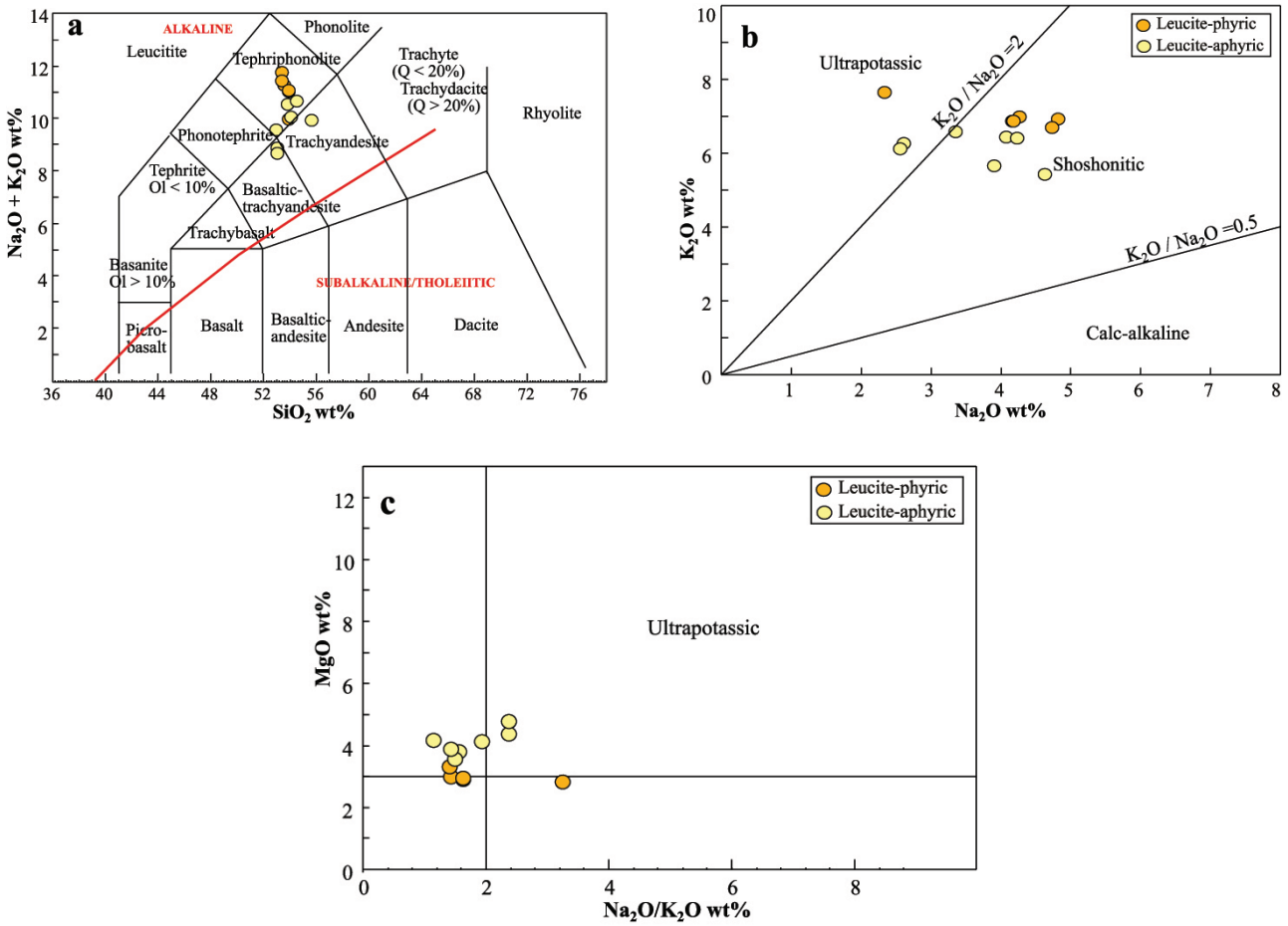


Figure 7. (a & b) K_2O vs. Na_2O and MgO vs. Na_2O/K_2O (Foley *et al.* 1987) for Kestanbol/Ezine leucite-phyric and leucite-aphyric dykes and **(c)** total alkalis vs. SiO_2 (Le Bas *et al.* 1986). The division between the alkaline and subalkaline fields defined by Irvine & Baragar (1971) has also been plotted onto the TAS diagram (red line). Samples recalculated to 100% on a H_2O- and CO_2-free basis.

basaltic-trachyandesite field (Figure 7c). According to the classification of ultrapotassic rocks proposed by Foley *et al.* (1987) and Foley (1992, 1994), the dyke samples resemble rocks of the Roman Province, Italy, and potassic-ultrapotassic volcanic rocks of Western Anatolia (Figure 8).

All dyke samples show an orogenic geochemical signature (Lustrino & Wilson 2007; Lustrino *et al.* 2011) with enrichment in large ion lithophile elements (LILEs; Cs, Rb, Ba and K) and deep troughs in high field strength elements (HFSEs; e.g., Nb and Ta) as well as Sr and Ti (Figure 9a). The parental melt of the tephriphonolite dykes was enriched in LILEs relative to HFSEs, compared to Miocene basanites of the Biga Peninsula that have an anorogenic geochemical signature similar to ocean island basalts (OIBs) (Aldanmaz *et al.* 2000; 2005) (Figure 9b). The tephriphonolite dykes show chondrite-normalised rare earth element (REE) patterns that are enriched in light REEs (LREEs) relative to heavy REEs (HREEs, Figure 9b) with $(La/Yb)_{CN}$ values ranging from 27.0 to 38.6 and slightly negative Eu anomalies ($Eu/Eu^* = 0.7$-0.8). The strong HREE depletion in the samples might indicate the presence of residual garnet in the mantle source.

Trace elements of the dykes are compared below with volcanic rocks from the Roman Magmatic Province. The Roman Province (e.g., Conticelli *et al.* 2002, 2009; Boari *et al.* 2009a; Gaeta *et al.* 2011) comprises ultrapotassic leucite-bearing volcanics formed by partial melting of a heterogeneous mantle source, infiltrated by phlogopite-rich veins resulting from the interaction of slab-derived melts and fluids with ambient mantle (Gaeta *et al.* 2011; Lustrino *et al.*, 2011 and references therein). The multi-element pattern of the dykes shows distinctive enrichment of Rb, Ba, Th and U; enrichment in Pb over Ce; and depletion of Nb and Ta when compared with OIB. The trace element pattern of the samples overlaps with the field of volcanic rocks from Roman Magmatic Province (data from Peccerillo 2005) and potassic-ultrapotassic

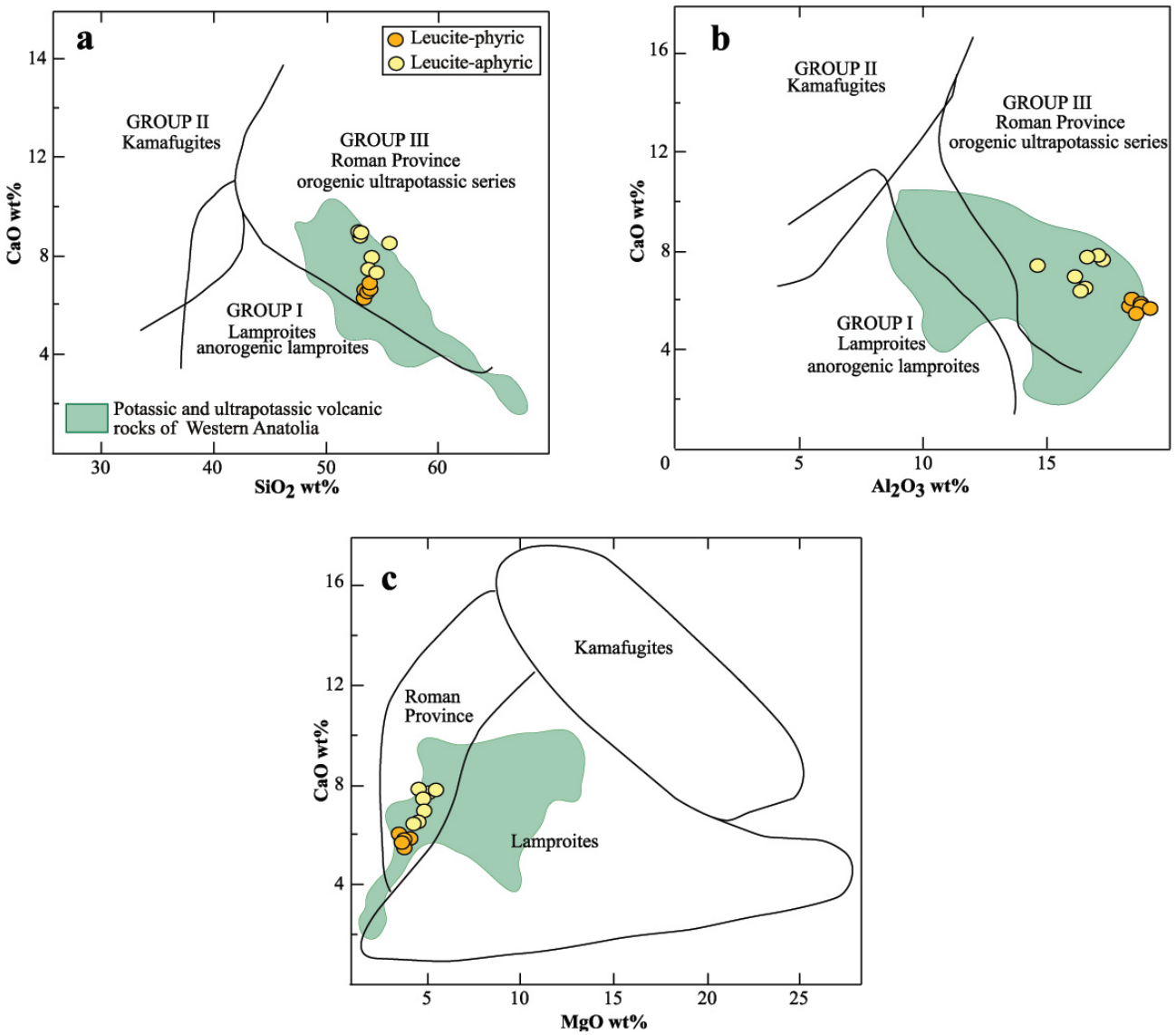


Figure 8. Plots of shoshonitic-ultrapotassic dykes on Group I, II and III ultrapotassic rock classification diagrams of Foley *et al.* (1987) and Foley (1992, 1994). Data source for Western Anatolian potassic-ultrapotassic volcanic rocks from Çoban & Flower (2006, 2007), Prelevic *et al.* (2010, 2012), Akal (2008) and Ersoy *et al.* (2008). Dyke samples are plotted on a water-free basis.

volcanic rocks of Western Anatolia (Prelevic *et al.* 2012). Enrichment in Cs, Rb, Ba and Pb and depletion in Nb, Ta and Ti usually indicate the presence of a subduction-modified mantle source. Such modifying influence can take place by sediment addition and mantle metasomatism (Foley *et al.* 1987; Sun & McDonough 1989; Wilson 1989; Pearce & Stern 2006). The geochemical pattern of the dykes closely resembles those of the global subducting sediment (GLOSS) of Plank & Langmuir (1998), providing further evidence for a crust-derived sediment addition to the mantle source. A distinctive positive Pb peak also suggests that a crustal component was present in the mantle source (Taylor & McLennan 1985, 1988). Finally, extreme Th enrichment and high Th/Yb and Th/La ratios (up to 1.1) are also considered to reflect contributions from subducted sediment to the mantle source (Rogers *et al.* 1985; Plank 2005). The high Sr/Nd ratios indicate carbonate addition from subducted oceanic lithosphere (Boari *et al.* 2009a). On a world-wide scale potassic and shoshonitic rocks can form in a number of tectonic settings (Müller *et al.* 1992). The tephriphonolite dykes exhibit a potassic postcollisional arc signature and overlap with postcollisional potassic ultrapotassic volcanic rocks of Western Anatolia (Figure 10).

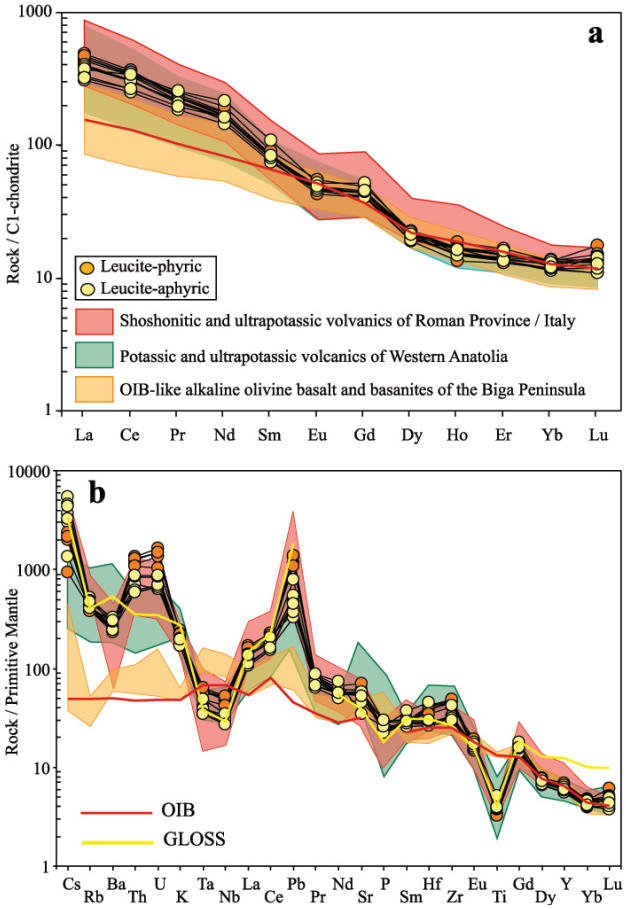


Figure 9. (a) Primitive mantle normalised trace element patterns and **(b)** chondrite-normalised REE patterns for the leucite-phyric and leucite-aphyric tephriphonolite dykes. Normalised values and OIB composition from Sun & McDonough (1989). GLOSS-global subducting sediment composition from Plank & Langmuir (1998). Data for Roman Magmatic Province from Peccerillo (2005). OIB-type alkali basalt and basanites of the Biga Peninsula from Aldanmaz *et al.* (2002, 2005). Data sources for Western Anatolian potassic-ultrapotassic volcanic rocks are given in Figure 8.

6. Ar-Ar Geochronology

$^{40}Ar/^{39}Ar$ isotope analyses were conducted on biotite and leucite crystals from fresh leucite phenocryst-bearing tephriphonolite dyke samples.

The fairly flat age spectra of biotite and leucite provide plateau ages of 21.22 ± 0.09 Ma and 22.21 ± 0.07 Ma, respectively (Figure 11 and Table 2). The $^{40}Ar/^{39}Ar$ ages are in line with the 21.5 ± 1.6 Ma ($^{87}Rb/^{86}Sr$ biotite) and 22.3 ± 0.2 Ma ($^{40}Ar/^{39}Ar$ biotite) – 22.8 ± 0.2 Ma ($^{40}Ar/^{39}Ar$ hornblende) ages of the Kestanbol Pluton reported by Birkle & Satır (1995) and Altunkaynak *et al.* (2012).

7. Discussion and Conclusion

Northward subduction of the northern branch of the Neo-Tethys Ocean from the late Cretaceous to the Tertiary was the mechanism responsible for convergence between the Anatolide-Tauride platform and the Sakarya continent (e.g., Şengör & Yılmaz 1981; Yılmaz 1981, 1990, 1997; Yılmaz *et al.* 1995; Delaloye & Bingöl 2000; Okay & Satır 2000, 2006). The collision boundary between these two plates is defined by the İzmir-Ankara-Erzincan Suture Zone. Subduction, collision and postcollisional extension gave rise to magmatic activities on the Biga Peninsula, which lasted from Eocene to Miocene times (Şengör & Yılmaz 1981; Yılmaz 1989, 1990; Güleç 1991; Harris *et al.* 1994; Karacık & Yılmaz 1998; Aldanmaz *et al.* 2000; Altunkaynak & Dilek 2006; Altunkaynak & Genç 2008; Dilek & Altunkaynak 2009; Yılmaz-Şahin *et al.* 2010; Altunkaynak *et al.* 2012). Based on previous studies (Karacık & Yılmaz 1998; Aldanmaz *et al.* 2000, 2006; Altunkaynak & Dilek 2006; Altunkaynak & Genç 2008; Dilek & Altunkaynak 2009; Altunkaynak *et al.* 2012 and references therein), magmatism on the Biga Peninsula can be summarised as follows: subduction of the Neo-Tethys Ocean caused metasomatism of the lithospheric mantle source via consumption and reworking of continental material. This metasomatised lithospheric mantle started to melt following slab breakoff and related asthenospheric upwelling between the Eocene and Oligo-Miocene. Uprise of asthenospheric material mitigated the subduction zone signature in the resulting volcanic rocks. This mantle source is characterised with high initial $^{87}Sr/^{86}Sr$ ratios (0.70757-0.70868) and low initial $^{143}Nd/^{144}Nd$ isotope ratios (0.51232-0.51246), as revealed in the early Miocene Kestanbol Pluton and associated high-K, shoshonitic volcanic rocks. Magmatism took place in a postcollisional extension regime and lasted from the late Oligocene to the Early Miocene.

The tephriphonolite dykes geochemically resemble the early Miocene plutons of the Biga Peninsula. Fingerprints of the subduction-related enrichment processes are clearly seen in plutonic, subvolcanic and volcanic rock of the Biga Peninsula (Figure 12a). All these rocks are characterised by different amounts of enrichment of LILE, HFSE (i.e. Th, Hf, Zr, Ta, Nb, P, Ti) and Pb. These patterns closely resemble the average continental crust (Rudnick & Fountain 1995; Taylor & McLennan 1985, 1988), indicating sediment recycling into the upper mantle through subduction (Elliott *et al.* 1997).

Di Vincenzo & Rocchi (1999) mentioned that the Nb/Yb ratios provide an estimate of source enrichment prior to the introduction of the subduction component. N-MORB normalised Nb/Yb ratios of the dykes are between 12.5 and 22.7, implying the contribution of a subduction component in the subcontinental lithospheric mantle. On

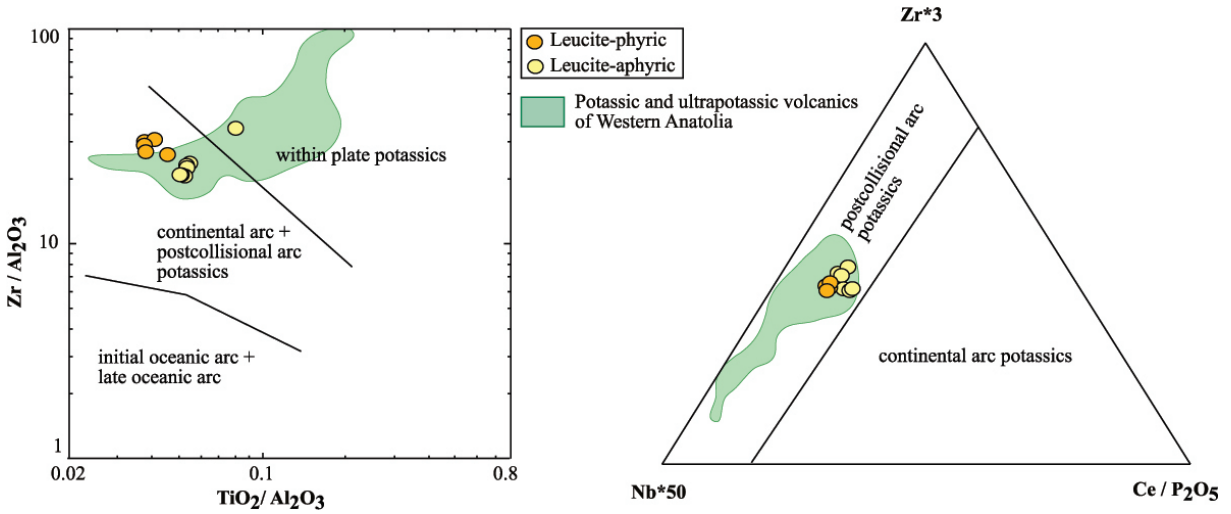


Figure 10. Tectonic setting of leucite-phyric and leucite-aphyric dykes in the discrimination diagrams of Müller *et al.* (1992) proposed for potassic volcanic rocks. The tephriphonolite samples overlap orogenic or subduction-related collisional potassic and ultrapotassic rocks of Western Anatolia (data sources for Western Anatolian potassic-ultrapotassic volcanics rocks are given in Figure 8).

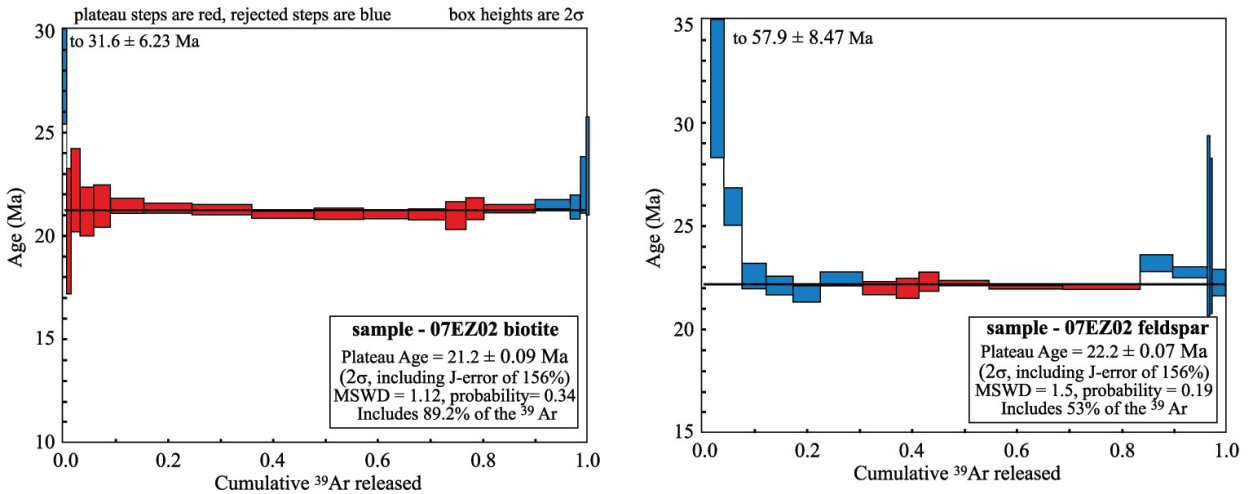


Figure 11. Apparent age spectrum for the dated leucite (pseudomorphic K-feldspar) and biotite crystals from a leucite-phyric tephriphonolite dyke.

the Th/Yb vs. Ta/Yb diagram, Ezine samples plot far above the mantle array, together with rocks from the Roman Magmatic Province rocks, and close to the upper crust composition. The tephriphonolite dykes are similar to, or even more enriched than, Western Anatolian potassic and ultrapotassic rocks, demonstrating the striking influence of the subducted sedimentary melt component in the lithospheric mantle source (Figure 13). The high Th/La and Th/Nb ratios of the dykes also reflect slab sediment recycling into an upper mantle source at a subduction zone (Plank 2005). Recycling of carbonate-bearing pelites (sedimentary carbonate) or limestone play an important role in the Roman Magmatic Province, controlling the genesis of silica-undersaturated leucite-bearing magmas (Thomsen & Schmidt 2008; Avanzinelli *et al.* 2009 and references therein; Boari *et al.* 2009a, 2009b; Conte *et al.* 2009). The tephriphonolite dykes with high Sr/Nd ratios can be related to sedimentary carbonate recycling from a carbonate-rich sedimentary component, instead of from pure sedimentary carbonates. Pure sedimentary carbonates are expected to behave as refractory phases at the sub-arc depths (Boari *et al.* 2009b and references therein).

The tephriphonolite dykes from the Biga Peninsula and mafic dykes described by Şahin-Yılmaz *et al.* (2010) stress the significance of K-bearing minerals in the mantle source

Table 2. Analytical data for $^{40}Ar/^{39}Ar$ age determinations from leucite-phyric tephriphonolite dykes using pseudomorphic leucite and biotite crystals (coordinates of sample 07EZ02 is 35 S 0437234 - 4402918).

Heating Step	$^{40}Ar/^{39}Ar$	$^{37}Ar/^{39}Ar$	$^{36}Ar/^{39}Ar$	Ca/K	% $^{40}Ar_A$	Cum $^{39}Ar_K$	Age (2σ) (Ma)
Sample: 07EZ02 biotiteMass: 1.412 mg; J = 0.003832 ± 0.000006							
1	1340.100	0.555	4.542	1.088	100.1	0.001	-13.8 ± 60.80
2	145.603	0.102	0.477	0.201	96.8	0.005	31.6 ± 6.23
3	73.001	0.066	0.237	0.129	96.0	0.013	20.3 ± 2.99
4	25.683	0.036	0.076	0.070	87.4	0.031	22.2 ± 1.99
5	13.881	0.028	0.037	0.056	77.7	0.057	21.2 ± 1.16
6	12.021	0.025	0.030	0.049	74.0	0.088	21.5 ± 1.01
7	9.454	0.027	0.021	0.052	66.9	0.152	21.5 ± 0.35
8	6.929	0.029	0.013	0.057	55.1	0.245	21.4 ± 0.24
9	5.372	0.024	0.008	0.048	42.2	0.358	21.3 ± 0.25
10	5.160	0.019	0.007	0.038	40.5	0.478	21.1 ± 0.18
11	4.553	0.019	0.005	0.038	32.4	0.571	21.1 ± 0.26
12	4.250	0.017	0.004	0.034	27.7	0.657	21.1 ± 0.24
13	4.468	0.020	0.005	0.039	31.1	0.728	21.1 ± 0.26
14	4.236	0.020	0.004	0.039	27.6	0.766	21.0 ± 0.67
15	4.086	0.018	0.003	0.034	23.8	0.800	21.4 ± 0.53
16	4.324	0.016	0.004	0.032	28.0	0.897	21.4 ± 0.19
17	4.125	0.023	0.003	0.045	23.7	0.965	21.6 ± 0.22
18	4.348	0.046	0.004	0.090	28.1	0.985	21.4 ± 0.57
19	4.581	0.096	0.004	0.189	28.4	0.994	22.5 ± 1.33
20	5.669	0.029	0.008	0.056	39.9	1.000	23.4 ± 2.34

Plateau age = 21.22 ± 0.09 Ma (2σ, including J-error of 0.156%)
MSWD = 1.12, probability = 0.34; includes 89.2% of the ^{39}Ar, steps 3 through 16

Heating Step	$^{40}Ar/^{39}Ar$	$^{37}Ar/^{39}Ar$	$^{36}Ar/^{39}Ar$	Ca/K	% $^{40}Ar_A$	Cum $^{39}Ar_K$	Age (2σ) (Ma)
Sample: 07EZ02 feldsparMass: 1.650 mg; J = 0.003832 ± 0.000006							
1	-7455.480	-1.507	-24.914	-2.950	98.7	0.000	-798.3 ± 201.9
2	2844.210	1.138	9.443	2.232	98.1	0.002	339.8 ± 67.06
3	366.909	0.292	1.213	0.572	97.7	0.015	57.9 ± 8.47
4	107.229	0.152	0.347	0.298	95.5	0.039	33.1 ± 4.75
5	33.049	0.126	0.099	0.247	88.5	0.075	26.0 ± 0.89
6	11.258	0.132	0.027	0.259	70.7	0.121	22.7 ± 0.60
7	7.909	0.154	0.016	0.301	59.1	0.173	22.2 ± 0.45
8	5.301	0.204	0.007	0.400	40.0	0.224	21.8 ± 0.39
9	5.196	0.153	0.007	0.300	36.8	0.305	22.6 ± 0.32
10	4.497	0.137	0.004	0.269	28.4	0.370	22.1 ± 0.31
11	4.230	0.091	0.003	0.178	23.9	0.412	22.1 ± 0.48
12	4.192	0.090	0.003	0.177	22.1	0.449	22.4 ± 0.46
13	4.073	0.343	0.003	0.673	20.1	0.547	22.3 ± 0.12
14	3.780	0.290	0.002	0.569	14.6	0.687	22.2 ± 0.09
15	3.669	0.121	0.002	0.238	11.9	0.835	22.2 ± 0.12
16	4.254	0.107	0.003	0.210	20.1	0.898	23.3 ± 0.41
17	3.895	0.059	0.002	0.115	14.5	0.964	22.8 ± 0.26
18	4.144	0.186	0.002	0.365	11.8	0.968	25.1 ± 4.32
19	4.012	0.150	0.002	0.293	10.6	0.973	24.6 ± 3.71
20	3.631	0.041	0.001	0.080	10.2	1.000	22.4 ± 0.63

Plateau age = 22.21 ± 0.07 Ma (2σ, including J-error of 0.156%)
MSWD = 1.5, probability = 0.19; includes 53% of the ^{39}Ar, steps 9 through 14

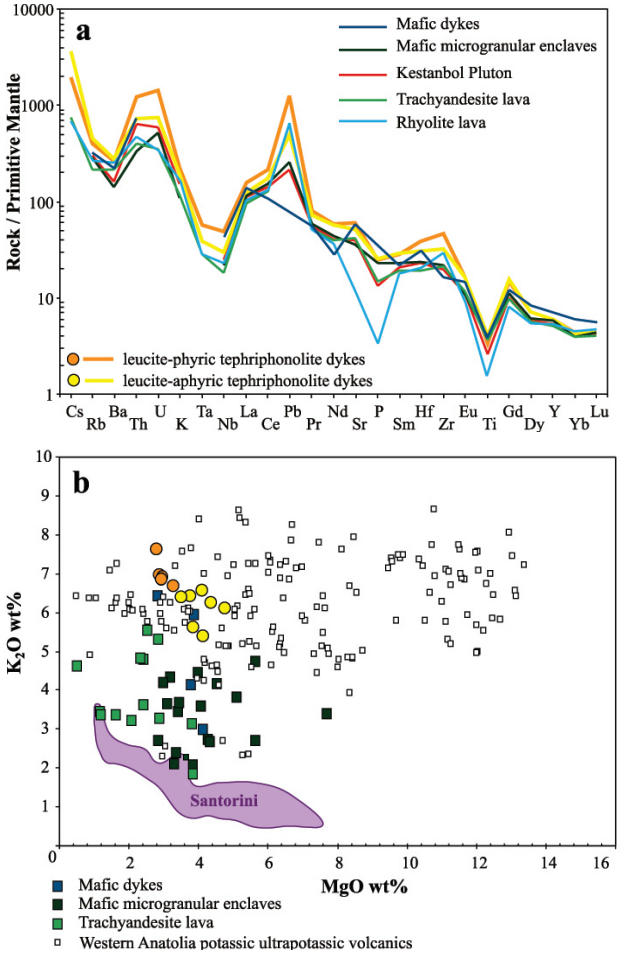


Figure 12. **(a)** Mantle-normalised (Sun & McDonough 1989) multi-element spider diagram for the Kestanbol Pluton, mafic microgranular enclaves and mafic dykes, average compositions of trachyandesites and rhyolites (data from Yılmaz 1989; Karacık & Yılmaz 1998; Aldanmaz *et al.* 2000; Yılmaz-Şahin *et al.* 2010) and average composition of leucite-bearing and leucite-free tephriphonolite dykes. **(b)** MgO vs. K_2O (wt %) for volcanic rocks from Biga Peninsula compared with potassic and ultrapotassic rocks of Western Anatolia (data sources given in Figure 8). Field of Santorini used as proxy for the melts derived from the mantle wedge above active oceanic-crust subduction.

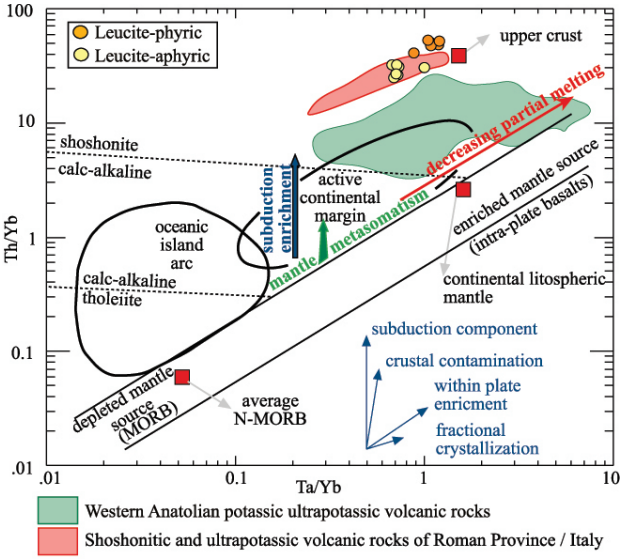


Figure 13. Th/Yb versus Ta/Nb diagram (Pearce 1983). Both types of tephriphonolite dykes are characterised by high Th/Yb relative to Ta/Nb ratios and closely resemble those of a mantle source modified by subduction, metasomatism and crustal contamination. Data for Western Anatolian volcanic rocks from Aldanmaz *et al.* 2000; Erkül *et al.* 2005; Innocenti *et al.* 2005; Çoban & Flower 2006 and 2007; Akal 2008; Ersoy *et al.* 2008; Ersoy *et al.* 2010; Karaoğlu *et al.* 2010; Prelevic *et al.* 2010 and 2012. Data for Roman Magmatic Province from Peccerillo (2005).

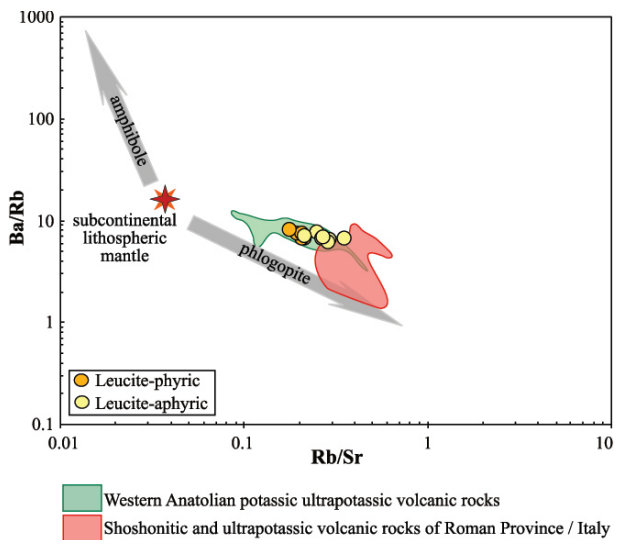


Figure 14. Tephriphonolite dykes overlap ultrapotassic (lamproite) rocks of Western Anatolia with their low Ba/Rb vs. high Rb/Sr ratios indicating presence of phlogopite in their mantle source. Subcontinental lithospheric mantle composition from McDonough (1990).

beneath Western Anatolia (Figure 12b). Tommasini *et al.* (2011) use Ba/Rb vs. Rb/Sr ratios to separate compositional variation due to amphibole vs. phlogopite metasomatism on within-plate and Tethyan realm lamproites and ultrapotassic rocks (Figure 14). The tephriphonolite dykes overlap ultrapotassic rocks from Western Anatolia and the Roman Magmatic Province and have high Rb/Sr and low Ba/Rb ratios, suggesting the presence and major role of phlogopite in their lithospheric mantle source rather than amphibole.

Field, geochronological and geochemical studies produce the following conclusions: 1) during northward subduction of northern branch of the Neo-Tethys Ocean, the lithospheric mantle source was metasomatised by subducted sediments; 2) the shoshonitic to ultrapotassic dykes were derived by partial melting of a previously

metasomatised and phlogopite-bearing subcontinental lithospheric mantle source, which shows sedimentary carbonate recycling from subducted oceanic lithosphere; 3) slightly younger ultrapotassic shoshonitic dykes intruded into the Kestanbol monzonite-granodiorite host rock and the metasediments of the Ezine group during the early Miocene (21.22 ± 0.09 Ma, 22.21 ± 0.07 Ma); 4) field and age relations between the Kestanbol monzonite-granodiorite and the dykes suggest coeval emplacement during postcollisional, orogenic magmatism on the Biga Peninsula; 5) the geochemical properties of the tephriphonolite dykes confirm that similarities exist between the volcanic products of the Roman Magmatic Province and Western Anatolian potassic-ultrapotassic rocks.

Acknowledgements

I am very grateful to Dr Dejan Prelevic and Dr P Van den Bogaard, who carried out the $^{40}Ar/^{39}Ar$ age analyses. Wolfgang Siebel and two anonymous referees are thanked for their valuable comments and contributions, which greatly improved the paper.

References

Akal, C. 2008. K-richterite-olivine-phlogopite-diopside-sanidine lamproites from the Afyon Volcanic Province, Turkey. *Geological Magazine* **145**, 1-16.

Akal, C., Candan, O., Koralay, O.E., Oberhänsli, R. Chen, F. & Dejan, P. 2012. Early Triassic potassic volcanism in the Afyon Zone of the Anatolides/Turkey: implications for the rifting of the Neo-Tethys. *International Journal of Earth Sciences (Geologische Rundschau)* **101**, 177-194.

Akal, C., Koralay, O.E., Candan, O., Oberhänsli, R. & Chen, F. 2011. Geodynamic significance of the early Triassic Karaburun granitoid (Western Turkey) for the opening history of Neo-Tethys. *Turkish Journal of Earth Sciences* **20**, 255-271.

Aldanmaz, E. 2002. Mantle source characteristics of alkali basalts and basanites in an extensional intracontinental plate setting, western Anatolia, Turkey: implications for multi-stage melting. *International Geological Review* **44**, 440-457.

Aldanmaz, E., Gourgaud, A. & Kaymakcı, N. 2005. Constraints on the composition and thermal structure of the upper mantle beneath NW Turkey: Evidence from mantle xenoliths and alkali primary melts. *Journal of Geodynamics* **39**, 277-316.

Aldanmaz, E., Köprübaşı, N., Gürer, O.F., Kaymakcı, N. & Gourgaud, A. 2006. Geochemical constraints on the Cenozoic, OIB-type alkaline volcanic rocks of NW Turkey: implications for mantle sources and melting processes. *Lithos* **86**, 50-76.

Aldanmaz, E., Pearce, J.A., Thirlwall, M.F. & Mitchell, J.G. 2000. Petrogenetic evolution of Late Cenozoic, post-collision volcanism in western Anatolia, Turkey. *Journal of Volcanology and Geothermal Research* **102**, 67-95.

Altunkaynak, Ş., Dilek, Y., 2006. Timing and nature of postcollisional volcanism in western Anatolia and geodynamic implications. In: Dilek, Y. & Pavlides, S. (eds.), *Postcollisional Tectonics and Magmatism in the Mediterranean Region and Asia*. Geological Society of America Special Paper, **409**, 321-351.

Altunkaynak, Ş., Dilek, Y., Genç, C.Ş., Sunal, G., Gertisser, R., Furnes, H., Foland, K.A. & Yang, J. 2012. Spatial, temporal and geochemical evolution of Oligo–Miocene granitoid magmatism in western Anatolia, Turkey. *Gondwana Resarch*, **21**, 961-986.

Altunkaynak, Ş. & Genç, C. 2008. Petrogenesis and time-progressive evolution of the Cenozoic continental volcanism in the Biga Peninsula, NW Anatolia (Turkey). *Lithos* **102**, 316-340.

Avanzinelli, R., Lustrino, M., Mattei, M., Melluso, L. & Conticelli, S. 2009. Potassic and ultrapotassic magmatism in the circum-Tyrrhenian region: Significance of carbonated pelitic vs. pelitic sediment recycling at destructive plate margins. *Lithos* **113**, 213-227.

Beccaletto, L. & Jenny, C. 2004. Geology and correlation of the Ezine Zone: A Rhodope fragment in NW Turkey. *Turkish Journal of Earth Sciences* **13**, 145-176.

Birkle, P. & Satır, M. 1992. Petrology, geochemistry and geochronology of a quartz-monzonite intrusion (Kestanbol granite) and their host rocks near Ezine, Biga-peninsula, NW Anatolia, Turkey. *ISGB-92 Abstracts* 44–45.

Birkle, P. & Satır, M. 1995. Dating, geochemistry and geodynamic significance of the tertiary magmatism of the Biga Peninsula, NW Turkey. *In*: Erler, A., Ercan, T., Bingöl, E. & Örçen, S. (eds.), *The Geology of the Black Sea Region*, Directorate of Mineral Research and Exploration, Ankara, 171-180.

Boari, E., Avanzinelli, R., Melluso, L., Giordano, G., Mattei, M., De Benedetti, A.A., Morra, V. & Conticelli, S. 2009a. Isotope geochemistry (Sr–Nd–Pb) and petrogenesis of leucite-bearing volcanic rocks from Colli Albani volcano, Roman Magmatic Province, Central Italy: inferences on volcano evolution and magma genesis. *Bulletin of Volcanology* **71**, 977-1005.

Boari, E., Tommasini, S., Laurenzi, M.A. & Conticelli, S. 2009b. Transition from ultrapotassic kamafugitic to sub-alkaline magmas: Sr, Nd, and Pb Isotope, trace element and ^{40}Ar-^{39}Ar age data from the Middle Latin Valley volcanic field, Roman Magmatic Province, Central Italy. *Journal of Petrology* **50**, 1327-1357.

Borsi, S., Ferrara, G., Innocenti, F. & Mazuoli, R. 1972. Geochronology and petrology of recent volcanics in the eastern Aegean Sea. *Bulletin Volcanologique* **36**, 473-496.

Brinkmann, R. 1966. Geotektonische Gliederung von Westanatolien. *Neues Jahrbuch für Geologie und Paläontologie-Monatshefte* **10**, 603-618.

Conte M.A., Dolfi, D., Gaeta, M., Misiti, V., Mollo, S. & Perinelli, C. 2009 Experimental constraints on evolution of leucite-basanite magma at 1 and 10^{-4} GPa: implications for parental compositions of Roman high-potassium magmas. *European Journal of Mineralogy* **21**, 763-782.

Conticelli, S., D'Antonio, M., Pinarelli, L. & Civetta, L. 2002. Source contamination and mantle heterogeneity in the genesis of Italian potassic and ultrapotassic volcanic rocks: Sr–Nd–Pb isotope data from Roman Province and Southern Tuscany. *Mineralogy and Petrology* **74**, 189-222.

Conticelli, S., Marchionni, S., Rosa, D., Giordano, G., Boari, E., Avanzinelli, R. 2009. Shoshonite and sub-alkaline magmas from an ultrapotassic volcano: Sr-Nd-Pb isotope data on the Roccamonfina volcanic rocks, Roman Magmatic Province, Southern Italy. *Contributions to Mineralogy and Petrology* **157**, 41-63.

Cox, K.G., Bell, J.D. & Pankhurst, R.J. 1979. *The Interpretation of Igneous Rocks*. George Allen & Unwin, London.

Çoban, H. & Flower, M.F.J. 2006. Mineral phase compositions in silica-undersaturated 'leucite' lamproites from the Bucak area, Isparta, SW Turkey. *Lithos* **89**, 275-299.

Çoban, H. & Flower, M.F.J. 2007. Late Pliocene lamproites from Bucak, Isparta (southwestern Turkey): Implications for mantle 'wedge' evolution during Africa-Anatolian plate convergence. *Journal of Asian Earth Sciences* **29**, 160-176.

Dalrymple, G.B. & Duffield, W.A. 1988. High Precision $^{40}Ar/^{39}Ar$ Dating of Oligocene Rhyolites from the Mogollon-Datil Volcanic Field Using a Continuous Laser System. *Geophysical Research Letters* **15**, 463-466.

Delaloye, M. & Bingöl, E. 2000. Granitoids from Western and Northwestern Anatolia: geochemistry and modeling of geodynamic evolution. *International Geology Review* **42**, 241-268.

Dilek, Y. & Altunkaynak, S. 2009. Geochemical and temporal evolution of Cenozoic magmatism in western Turkey: Mantle response to collision, slab breakoff, and lithospheric tearing in an orogenic belt. In: Van Hinsbergen, D.J.J., Edwards, M.A. & Govers, R. (eds.), *Collision and Collapse at the Africa–Arabia–Eurasia Subduction Zone*. Geological Society, Special Publications **311**, 213-233.

Di Vincenzo, G. & Rocchi, S. 1999. Origin and interaction of mafic and felsic magmas in an evolving late orogenic setting: The early Paleozoic Terra Nova intrusive complex, Antarctica. *Contributions to Mineralogy and Petrology* **137**, 15-35.

Elliott, T., Plank, T., Zindler, A., White, W. & Bourdon, B. 1997. Element transport from slab to volcanic front at the Mariana arc. *Journal of Geophysical Research* **102**, 14991-15019.

Ercan, T., Satir, M., Steinitz, G., Dora, A., Sarıfakioğlu, E., Adis, C., Walter, H.J. & Yıldırım, T. 1995. Biga Yarımadası ile Gökçeada, Bozcaada ve Tavşan adalarındaki (KB Anadolu) Tersiyer volkanizmasının özellikleri [Characteristics of the Tertiary volcanism of the Biga Peninsula, Gökçeada, Bozcaada and Tavşanadası NW Anatolia]. *Bulletin of the Mineral Research and Exploration Institute of Turkey* **117**, 55-86 [in Turkish with English abstract].

Erkul, F., Helvacı, C. & Sozbilir, H. 2005. Stratigraphy and geochronology of the Early Miocene volcanic units in the Bigadic borate basin, western Turkey. *Turkish Journal of Earth Sciences* **14**, 227-253.

Ersoy, Y., Helvacı, C., Sözbilir, H., Erkül, F. & Bozkurt, E. 2008. A geochemical approach to Neogene-Quaternary volcanic activity of western Anatolia: An example of episodic bimodal volcanism within the Selendi Basin, Turkey. *Chemical Geology* **255**, 265-282.

Ersoy, E.Y., Helvacı, C. & Palmer, M.R. 2010. Mantle source characteristics and melting models for the early-middle Miocene mafic volcanism in Western Anatolia: implications for enrichment processes of mantle lithosphere and origin of K-rich volcanism in post-collisional settings. *Journal of Volcanology and Geothermal Research* **198**, 112-128.

Foley, S.F. 1992. Petrological characterization of the source components of potassic magmas: geochemical and experimental constraints. *Lithos* **28**, 187-204.

Foley, S.F. 1994. Geochemische und experimentelle Untersuchungen zur Genese der kalireichen Magmatite. *Neues Jahrbuch für Mineralogie-Abhandlungen* **167**, 1-55.

Foley, S.F., Venturelli, G., Green, D.H. & Toscani, L. 1987. The ultrapotassic rocks: characteristics, classification and constraints for petrogenetic models. *Earth Science Reviews* **24**, 81-134.

Fytikas, M., Giuliani, O., Innocenti, F., Marinelli, G. & Mazzuoli, R. 1976. Geochronological data on recent magmatism of the Aegean Sea. *Tectonophysics* **21**, 29-34.

Gaeta, M., Freda, C., Marra, F., Di Rocco, T., Gozzi, F., Arienzo, I., Giaccio, B. & Scarlato, P. 2011 Petrology of the most recent ultrapotassic magmas from the Roman Province (Central Italy). *Lithos* **127**, 298-308.

Göncüoğlu M.C., Çapkınoğlu, S., Gürsü, S., Noble, P., Turhan, N., Tekin, U.K., Okuyucu, C. & Göncüoğlu, Y. 2007. The Mississippian in the Central and Eastern Taurides (Turkey): constraints on the tectonic setting of the Tauride-Anatolide Platform. *Geologica Carpathica* **58**, 427-442.

Göncüoğlu, M.C. & Kozlu, H. 2000. Early Paleozoic evolution of the NW Gondwanaland: Data from southern Turkey and surrounding regions. *Gondwana Research* **3**, 315-324.

Gözler, M.Z., Ergül, E., Akçaören, F., Genç, Ş., Akat, U. & Acar, Ü. 1984. Çanakkale Boğazı Doğusu-Marmara Denizi Güneyi-Bandırma-Balıkesir-Edremit ve Ege Denizi Arasındaki Bölgenin Jeolojisi [Geology of East of Dardanelles-South of Sea of Marmara-Bandırma-Balıkesir-Edremit and Aegean Sea]. Maden Tetkik ve Arama Enstitüsü Report No. **7430** [in Turkish, unpublished].

Güleç, N. 1991. Crust–mantle interaction in western Turkey: implications from Sr and Nd isotope geochemistry of Tertiary and Quaternary volcanics. *Geological Magazine* **128**, 417-435.

Harris, N.B.W., Kelley, S. & Okay, A.I. 1994. Post-collisional magmatism and tectonics in northwest Anatolia. *Contributions to Mineralogy and Petrology* **117**, 241-252.

Innocenti, F., Agostini, T.S., Di Vincenzo, G., Doglioni, C., Manetti, P., Savaşçın, M.Y. & Tonarini, S. 2005. Neogene and Quaternary volcanism in Western Anatolia: Magma sources and geodynamic evolution. *Marine Geology* **221**, 397-421.

Irvine, T.N. & Baragar, W.R.A. 1971. A guide to the chemical classification of the common volcanic rocks. *Canadian Journal of Earth Sciences* **8**, 523-448.

Kalafatcıoğlu, A. 1963. Geology around Ezine and Bozcaada, the age of the limestones and serpentinites. *Maden Tetkik ve Arama (MTA) Dergisi* **60**, 61-70.

Karacik, Z. 1995. *Ezine-Ayvacık (Çanakkale) Dolayında Genç Volkanizma-plütonizma İlişkileri* [Relationship Between Young Volcanism and Plutonism in Ezine-Ayvacık (Çanakkale) Region]. PhD Thesis, İstanbul Technical University, İstanbul-Turkey [in Turkish with English abstract, unpublished].

Karacık, Z. & Yılmaz, Y. 1998. Geology of ignimbrites and the associated volcano-plutonic complex of the Ezine area, northwestern Anatolia. *Journal of Volcanology and Geothermal Research* **85**, 251-264.

Karaoğlu, Ö., Helvaci, C. & Ersoy, Y. 2010. Petrogenesis and $^{40}Ar/^{39}Ar$ geochronology of the volcanic rocks of the Usak-Güre basin, western Türkiye. *Lithos* **119**, 193-210.

Ketin, İ. 1966. Tectonic units of Anatolia (Asia Minor). *Bulletin of the Mineral Research and Exploration Institute (MTA) of Turkey* **66**, 20-34 [in Turkish with English abstract].

Le Bas, M.J., Le Maitre, R.W., Streckeisen, A. & Zanettin, B. 1986. Chemical classification of volcanic rocks based on the total alkali-silica diagram. *Journal of Petrology* **27**, 745-750.

Lustrino, M., Duggen, S. & Rosenberg, C.L. 2011. The central-western Mediterranean: Anomalous igneous activity in an anomalous collisional tectonic setting. *Earth-Science Reviews* **104,** 1-40.

Lustrino, M. & Wilson, M. 2007. The circum-Mediterranean anorogenic Cenozoic igneous province. *Earth-Science Reviews* **81**, 1-65.

McDonough, W.F. 1990. Constraints on the composition of the continental lithospheric mantle. *Earth and Planetary Science Letters* **101**, 1-18.

Müller, D., Rock, N.M.S. & Groves, D.I. 1992. Geochemical discrimination between shoshonitic and potassic volcanic rocks in different tectonic setting: a pilot study. *Mineralogy Petrology* **46**, 259-289.

Okay, A.İ. & Satir, M. 2000. Coeval plutonism and metamorphism in a latest Oligocene metamorphic core complex in northwest Turkey. *Geological Magazine* **137**, 495-516.

Okay, A.İ. & Satir, M. 2006. Geochronology of Eocene plutonism and metamorphism in northwest Turkey: evidence for a possible magmatic arc. *Geodinamica Acta* **19**, 251-266.

Okay, A.İ., Satır, M., Maluski, H., Siyako, M., Monie, P., Metzger, R. & Akyüz, S. 1996. Paleo- and Neo-Tethyan events in northwestern Turkey: Geologic and geochronologic constraints. In: Yin, A. & Harrison, M. (eds.), *The Tectonic Evolution of Asia*. Cambridge University Press, Cambridge, 420-441.

Okay, A.İ., Satır, M. & Siebel, W. 2006. Pre-Alpide orogenic events in the Eastern Mediterranean region. European Lithosphere Dynamics. *Geological Society, London, Memoirs* **32**, 389-405.

Okay, A.I., Siyako, M. & Bürkan, K.A. 1991. Geology and tectonic evolution of the Biga Peninsula. In: Dewey, J.F. (ed.), *Special Issue on Tectonics*, *Bulletin of the Technical University of Istanbul* **44**, 191-225.

Okay, A.İ. & Tüysüz, O. 1999. Tethyan sutures of northern Turkey. In: Durand, B., Jolivet, L., Horváth, F. & Séranne, M. (eds.), *The Mediterranean Basin: Tertiary Extension within the Alpine Orogen*. Geological Society of London, Special Publication **156**, 475-515.

Pearce, J.A. 1983. Role of sub-continental lithosphere in magma series at active continental margins. In: Hawkesworth, C.J. & Norry, M.J. (eds.), *Continental Basalts and Mantle Xenoliths*. Birkhauser, Basel, 230-249.

Pearce, J.A. & Stern, R.J. 2006. The origin of back-arc basin magmas: trace element and isotope perspectives. *AGU Geophysical Monograph Series* **166**, 63-86.

Peccerillo, A. 2005. *Plio-Quaternary Volcanism in Italy. Petrology, Geochemistry, Geodynamics*. Springer, Heidelberg.

Plank, T. 2005. Constraints from thorium/lanthanum on sediment recycling at subduction zones and the evolution of the continents. *Journal of Petrology* **46**, 921-944.

Plank, T. & Langmuir C.H. 1998. The chemical composition of subducting sediment and its consequences for the crust and mantle. *Chemical Geology* **145**, 325-394.

Prelević, D., Akal, C., Foley, S., Romer, R., Stracke, A. & Van Den Bogaard, P. 2012. Ultrapotassic mafic rocks as geochemical proxies for post-collisional dynamics of orogenic lithospheric mantle: the case of southwestern Anatolia, Turkey. *Journal of Petrology* **53**, 1019-1055.

Prelević, D., Akal, C., Romer, R. & Foley, S.F. 2010. Lamproites as indicators of accretion and/or shallow subduction in the assembly of Southwestern Anatolia, Turkey. *Terra Nova* **22**, 443-452.

Rogers, N.W., Hawkesworth, C.J., Parker, R.J. & Marsh, J.S. 1985. The geochemistry of potassic lavas from Vulsini, central Italy and implications for mantle enrichment processes beneath the Roman region. *Contributions to Mineralogy and Petrology* **90**, 244-257.

Rudnick, R.L. & Fountain, D.M. 1995. Nature and composition of the Continental Crust: a lower crustal perspective. *Review of Geophysics* **33**, 267-309.

Stampfli, G.M. 2000. Tethyan oceans. In: Bozkurt, E., Winchester, J.A. & Piper, J. D. A. (eds.), *Tectonics and Magmatism in Turkey and the Surrounding Area*. Geological Society of London, Special Publication **173**, 1-23.

Sun, S.S. & McDonough, W.F. 1989. Chemical and isotopic systematics of oceanic basalts; implications for mantle composition and processes. In: Saunders, A.D. & Norry, M.J. (eds.), *Magmatism in the Ocean Basins*. Geological Society of London, Special Publication No. **42**, 313-345.

Şengör, A.M.C. & Yılmaz, Y. 1981. Tethyan evolution of Turkey: a plate tectonic approach. *Tectonophysics* **75**, 181-241.

Taylor, S.R. & McLennan, S.M. 1985. *The Continental Crust: Its Composition and Evolution*. Blackwell, Oxford.

Taylor, S.R. & McLennan, S.M. 1988. The significance of the rare earths in geochemistry and cosmochemistry. In: Gschneidner, K.A. & Eyring, L. (eds.), *Handbook on the Physics and Chemistry of Rare Earths*. Elsevier, Amsterdam, 485-578.

Thomsen, T.B. & Schmidt, M.W. 2008. Melting of carbonated pelites at 2.5–5.0 GPa, silicate–carbonatite liquid immiscibility, and potassium–carbon metasomatism of the mantle. *Earth and Planetary Science Letters* **267**, 17-31.

Tommasini, S., Avanzinelli, R. & Conticelli, S. 2011. The Th/La and Sm/La conundrum of the Tethyan realm lamproites. *Earth and Planetary Science Letters* **301**, 469-478.

Van den Bogaard, P. 1995. $^{40}Ar/^{39}Ar$ ages of sanidine phenocrysts from Laacher See Tephra (12,900 yr BP): Chronostratigraphic and petrological significance. *Earth and Planetary Science Letters* **133,** 163-174.

Wilson, M. 1989. *Igneous Petrogenesis: A Global Tectonic Approach*. Chapman & Hall, London.

Yaltırak, C. & Okay, A.İ. 2004. Edremit Körfezi kuzeyinde Paleotetis birimlerinin jeolojisi. İTÜ Dergisi **3**, 67-79.

Yılmaz, Y. 1989. An approach to the origin of volcanic rocks of western Turkey. *Tectonic Evolution of Marmara Poly-Project, ETH Zurich*, 31-53.

Yılmaz, Y. 1990. Comparison of young volcanic associations of western and eastern Anatolia under compressional regime: a review. *Journal of Volcanology and Geothermal Research* **44**, 69-87.

Yılmaz, Y. 1997. Geology of Western Anatolia: active tectonics of northwestern Anatolia. *The Marmara Poly Project*. VDF, Hochschulverlag Ag An Der ETH, Zürich, 1-20.

Yılmaz, Y., Genç, Ş.C., Karacik, Z. & Altunkaynak, S. 2001. Two contrasting magmatic associations of NW Anatolia and their tectonic significance. *Journal of Geodynamics* **31**, 243-271.

Yılmaz, Y., Genç, Ş.C., Yiğitbaş, E., Bozcu, M. & Yılmaz, K. 1995. Geological evolution of the late Mesozoic continental margin of Northwestern Anatolia. *Tectonophysics* **243**, 155-171.

Yılmaz-Şahin, S., Örgün, Y., Güngör, Y., Göker, A.F., Gültekin, A.H. & Karacık, Z. 2010. Mineral and whole-rock geochemistry of the Kestanbol Granitoid (Ezine-Çanakkale) and its mafic microgranular enclaves in northwestern Anatolia: evidence of felsic and mafic magma interaction. *Turkish Journal of Earth Sciences* **19**, 101-122.